



LAWRENCE
LIVERMORE
NATIONAL
LABORATORY

ACTINIC MASK INSPECTION AT THE ALS: RISK REDUCTION ACTIVITIES FOR 2003

Anton Barty, Rick Levesque, Jay Ayers, Yanwei
Liu, Eric Gullikson, Paul Barale

January 5, 2004

Disclaimer

This document was prepared as an account of work sponsored by an agency of the United States Government. Neither the United States Government nor the University of California nor any of their employees, makes any warranty, express or implied, or assumes any legal liability or responsibility for the accuracy, completeness, or usefulness of any information, apparatus, product, or process disclosed, or represents that its use would not infringe privately owned rights. Reference herein to any specific commercial product, process, or service by trade name, trademark, manufacturer, or otherwise, does not necessarily constitute or imply its endorsement, recommendation, or favoring by the United States Government or the University of California. The views and opinions of authors expressed herein do not necessarily state or reflect those of the United States Government or the University of California, and shall not be used for advertising or product endorsement purposes.

This work was performed under the auspices of the U.S. Department of Energy by University of California, Lawrence Livermore National Laboratory under Contract W-7405-Eng-48.



EUV mask blank
inspection at the
ALS



ACTINIC MASK INSPECTION AT THE ALS

RISK REDUCTION ACTIVITIES FOR 2003

VNL EUV Mask Blank
Technology transfer program

21 December 2003

Submitted to:

Obert Wood
International SEMATECH
2706 Montopolis Drive
Austin, TX, 78741

CONTENTS

1	EXECUTIVE SUMMARY	3
2	SCOPE AND CONTEXT OF THIS REPORT	4
2.1	PROJECT BACKGROUND.....	4
2.2	TOP-LEVEL DESCRIPTION OF RISK REDUCTION TASKS.....	4
3	REPORT ON RISK REDUCTION ACTIVITIES.....	5
3.1	FABRICATION OF ZONE PLATE IMAGING OPTIC	5
3.1.1	<i>Overview of AIM imaging system.....</i>	<i>5</i>
3.1.2	<i>Zone plate design for AIM imaging.....</i>	<i>7</i>
3.1.3	<i>Zone plate fabrication.....</i>	<i>8</i>
3.2	IMAGING SUB-SYSTEM PROOF OF PRINCIPLE DEMONSTRATION	11
3.2.1	<i>AIM mode imaging test stand</i>	<i>11</i>
3.2.2	<i>Demonstration of imaging with resolution to 80nm dense lines</i>	<i>13</i>
3.3	10X OPTIC DEMONSTRATION	17
3.3.1	<i>Hardware fabrication and installation.....</i>	<i>17</i>
3.3.2	<i>Measurement of system throughput.....</i>	<i>20</i>
3.3.3	<i>Knife-edge tests of spot size.....</i>	<i>22</i>
3.4	DATA ACQUISITION SYSTEM AND ELECTRONICS	23
3.4.1	<i>Overview of data acquisition system.....</i>	<i>24</i>
3.4.2	<i>Demonstration of continuous real-time data acquisition</i>	<i>26</i>

This work was performed under the auspices of the U.S. Department of Energy by University of California Lawrence Livermore National Laboratory under contract No. W-7405-Eng-48 and University of California Lawrence Berkeley National Laboratory. This project is supported by International SEMATECH under Project Lith 343.

This document may contain research results which are experimental in nature. Neither the United States Government, nor any agency thereof, nor The Regents of the University of California, nor Sandia Corporation, nor any of their employees, makes any warranty, express or implied, or assumes any legal responsibility for the accuracy, completeness, or usefulness of any information, apparatus, product, or process disclosed, or represents that its use would not infringe privately owned rights. Reference to any specific commercial product, process, or service by its trade name, trademark, manufacturer, or otherwise, does not constitute or imply an endorsement or recommendation by the United States Government or any agency thereof, by The Regents of the University of California, or by Sandia Corporation. The views and opinions of authors expressed herein do not necessarily state or reflect those of the United States Government or any agency thereof, by The Regents of the University of California, or by the Sandia Corporation and shall not be used for advertising or product endorsement purposes.

1 EXECUTIVE SUMMARY

This document reports on risk reduction activities performed at the VNL during CY2003 as a part of the Lith-343 actinic inspection project funded by International SEMATECH. The risk reduction activities described in this document comprise deliverable items 3.1.3, 3.1.4, 3.1.5 and 3.1.6 of Amendment 6 to the VNL EUV mask blank technology transfer contract.

The following is a brief summary of the status of the risk reduction activities as at 22 December 2003.

3.1.3 Fabrication of zone plate imaging optic

Zone plates for use in the AIM mode imaging part of the tool have been fabricated and are ready to use. Two designs were fabricated: one set on a Silicon Nitride membrane, and one set of free-standing zone plates. SEM images of both the free-standing and supported zone plates indicate that they have been fabricated to the required specifications are included in this report.

3.1.4 Imaging sub-system proof of principle demonstration

A test-stand has been constructed to perform proof-of-principle tests of the zone plate optic using the reflectometer on Beamline 6.3.2 at the ALS. Tests of zone plate performance indicate spatial resolution down to 80nm dense lines on the mask (corresponding to 20nm dense lines at the wafer in a 4x reduction stepper). This is consistent with the anticipated resolution of the optic, which is 107nm based on the design specifications of 0.0625NA clear aperture at 6 degrees to the mask required to emulate stepper imaging in AIM mode. We believe higher resolution could be achieved with a different zone plate design not intended to emulate the imaging performance of a stepper system.

3.1.5 10x optic throughput demonstration

A test-stand has been constructed and installed on the actinic inspection beamline to test performance of the Schwarzschild optic in the configuration to be used in the final inspection system, including the pinhole chamber fold mirror assembly required in the final design. System throughput of the fold mirror and Schwarzschild optic has been measured, with throughput of the Schwarzschild optic measured to peak at 31% at 13.45nm. A slight mismatch in wavelength has been observed between the fold mirror and the Schwarzschild optic, decreasing the measured system throughput. This wavelength mismatch will be corrected by coating an additional fold mirror to improve performance of the final system. The Schwarzschild spot size was also measured using a knife-edge test, with a spot size of 1 μ m FWHM measured.

3.1.6 Data acquisition system and electronics

The ability to continuously collect and store two channels of analogue data at speed of 100kHz or greater is required for the inspection project. We have acquired data acquisition hardware capable of running at this speed, and demonstrated continuous acquisition of two channels of data at speeds of up to 500kHz for intervals in excess of 5 minutes continuous readout. The limiting factor on acquisition rate is computer speed, and we found no limit to acquisition time other than available disk space.

2 SCOPE AND CONTEXT OF THIS REPORT

2.1 Project background

The purpose of this project is to design an actinic mask inspection tool capable of operating in two modes: high-speed scanning for the detection of multilayer defects (inspection mode), and a high-resolution aerial image mode in which the image emulates the imaging illumination conditions of a stepper system (aerial image or AIM mode). The technical requirements of each of these modes of operation have been described in detail elsewhere, and can be summarised as follows:

Defect inspection mode

This mode of operation is designed to scan large areas of the mask for defects EUV multilayer coatings. The goal is to detect the presence of multilayer defects on a mask blank and to store the co-ordinates for subsequent review in AIM mode, thus it is not essential that the illumination and imaging conditions match that of a production stepper. Because of the low defect density achieved using current multilayer coating technology it is necessary to be able to efficiently scan large areas of the mask in order to obtain sufficient statistics for use in cross-correlation experiments. Speed of operation as well as sensitivity is therefore key to operation in defect inspection mode.

Aerial Image Microscope (AIM) mode

In AIM mode the tool is configured so that the collected data emulates the aerial image of a stepper system, thereby enabling rapid evaluation of mask defects and patterning without the need for a resist exposure step. An essential characteristic of operation in this mode is that the illumination and imaging conditions through focus should emulate as accurately as possible that of a production stepper system. This mode is designed for local review of defects over a small sub-field of the mask; therefore it is not necessary to have the same high-speed throughput required for defect inspection mode.

2.2 Top-level description of risk reduction tasks

As a part of this project, certain risk reduction tasks were to be completed in CY2003 to demonstrate progress towards construction of the complete inspection tool. Specifically this report addresses those deliverables detailed in the 2003-2004 statement of work dealing with risk-reduction activities to be completed in CY2003. The risk-reduction activities identified in the statement of work are:

3.1.7 Fabrication of zone plate imaging optic

The VNL will fabricate zone plate imaging elements for use in the upgraded inspection system when operating in high-resolution imaging mode in accordance with the design detailed at the system design review (3.1.2).

3.1.8 Imaging sub-system proof of principle demonstration

The VNL will conduct risk-reduction experiments to demonstrate the resolution of the zone-plate imaging sub-system to be used in the new inspection system using similar or identical optical imaging elements to those to be used in the final system, and will report on the resolution and efficiency, and compare the performance obtained with the predicted diffraction-limited spatial resolution targeted for this optic.

3.1.9 10x optic throughput demonstration

The VNL will integrate the 10x optic to be used in the final system into an interim vacuum chamber at the ALS. Both the throughput and spot size will be verified to be compatible with the requirements of the inspection project.

3.1.10 Data acquisition system and electronics

The VNL will purchase data acquisition and detector system components, substantially complete programming of the data acquisition system, and demonstrate operation using either simulated data or data obtained using the existing actinic inspection tool. The VNL will compare maximum data acquisition rate attained in the laboratory with the data rates planned for the final inspection system.

The purpose of this report is to detail progress in completion of these risk reduction activities. Each line item above is addressed in a separate section below.

3 REPORT ON RISK REDUCTION ACTIVITIES

3.1 Fabrication of zone plate imaging optic

The concept design for Aerial Imaging mode imaging involves using a zone plate optic to view features on the mask. During CY 2003 the required zone plates have been fabricated in the nanofabrication laboratory at LBL. The design of these zone plates is novel and specifically adapted for use in the actinic microscope, and therefore differs in design from the more traditional zone plates used in transmission microscopes. We therefore first discuss briefly the concept design for AIM mode imaging, then describe the results of zone plate fabrication. Initial experiments on characterising the performance of the zone plates is further discussed in a separate section below.

3.1.1 Overview of AIM imaging system

The purpose of the zone plate microscope is to provide some advanced capability for stepper-equivalent imaging of EUV masks in advance of the availability of commercial tools. In order to properly emulate the imaging characteristics of a 0.25NA 4x reduction lithography stepper it is necessary to have a pupil with a clear aperture of 0.0625NA observing the mask at an angle of incidence of 6°. In this way the zone plate optic will see the mask with the same conditions (angle of incidence, NA, wavelength and illumination) as the projection optics in the lithographic system, and should therefore provide an image that is close to that anticipated when the mask is printed in a lithographic system. The rationale behind this has been described in a previous LLNL report to ISMT on designs for an EUV aerial image microscope tool.

Zone plate microscopes typically operate in transmission mode with the condenser and imaging optics on opposite sides of the object. This relies on the object being transmissive, whilst EUV masks are reflective. In order to image a reflective EUV mask it is necessary to fold the system back on itself so that both the illumination and imaging optics are on the same side of the object. The desired mask-side aperture of 0.0625NA at 6° allows adequate clearance for both the

optics and illumination on the same side of the mask, although space is tight. The same problems are encountered when designing the mask-side of lithographic optics.

The simplest zone plate design contemplates a single imaging element (zone plate) imaging the mask with a 0.0625NA zone plate tilted with respect to the mask so that the optical axis of the imaging system is at 6° to the mask. The imaging system is therefore a tilted optical system and as such will suffer from keystone distortion and require a tilted image plane. The resultant image will suffer from distortion, and it will be difficult to maintain the whole field of view in focus at the same time.

An alternative design that can correct for the effects of imaging the mask at an angle is shown in Figure 1. By using an off-axis portion of an on-axis zone plate, so that the image is formed on an axis perpendicular to the mask as shown in Figure 1(a). In order to capture the marginal ray of the of an off-centre 0.0625NA AIM pupil centred on a chief ray angled at 6° to the mask it is necessary to have a parent zone plate with a numerical aperture of 0.166NA.

This design has the benefit of eliminating keystone distortion suffered by the tilted optic design, and results in object and image planes parallel to one another and the zone plate. A second advantage of adopting this design is that the zero and first order diffraction orders are physically separated, as shown in Figure 1(b), reducing flare in the system and allowing for more relaxed placement of the order sorting aperture (if required).

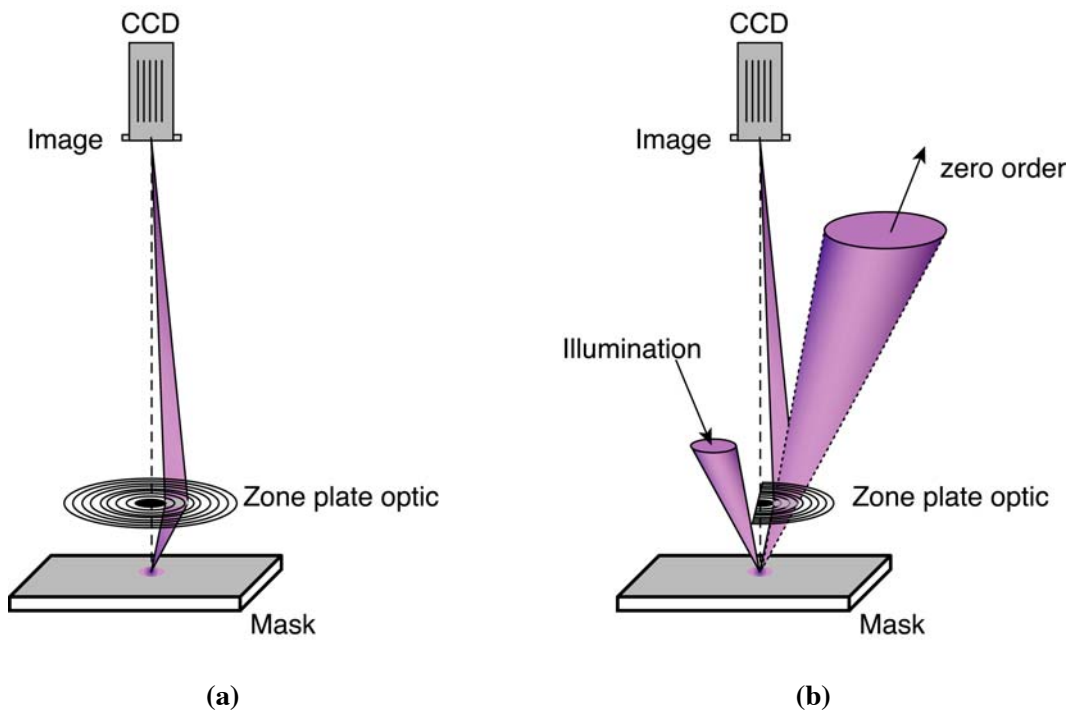


Figure 1

Conceptual layout of the zone plate imaging sub-system: (a) An off-axis portion of a 0.166NA parent zone plate is used to image the mask onto the CCD camera, keeping the whole field of view in focus and eliminating keystone distortion.

(b) To illuminate the mask, only that portion of the zone plate involved in imaging the mask is fabricated – the remainder is left unpatterned and may be used to introduce illumination into the system. Using the off-axis design has the added benefit of physically separating unwanted diffraction orders from the zone plate optic.

3.1.2 Zone plate design for AIM imaging

The design of a zone plate is completely specified by the wavelength, bandwidth and resolution (NA) of the optic. In particular we have the following standard relationships for zone plate design:

Outer zone width:	$\delta = \Delta r_N = \lambda/2NA$
Number of zones:	$N < \lambda/\Delta\lambda$
Focal length:	$f = 4N\Delta r_N^2/\lambda$
Diameter:	$D = 4N\Delta r_N$
Field of view:	$FOV \approx D/3$

For AIM mode imaging the NA of the optic is fixed and the wavelength is set at 13.5nm, leaving bandwidth as the only undetermined parameter. The allowable bandwidth for a zone plate is set by restrictions on the allowable chromatic aberration in the imaging system, and results from the fact that zone plates are a highly dispersive optic.

For a 6-mirror camera plus mask and condenser optics the bandwidth is anticipated to be 2%. This corresponds to a maximum of 50 zones in a zone plate, producing a zone plate with a very short ($24\mu\text{m}$) working distance and small field of view that is impractical for use in the proposed microscope.

We instead choose to operate with the beamline monochromator in place, providing between 0.05% and 0.1% illumination bandwidth depending on exit slit settings. This enables the use of up to 2000 zones in the zone plate producing a focal length close to 1mm. This enables the zone plate to be held 1mm from the mask, reducing the risk of accidental contact with the mask surface. Based on the desired wavelength, and the design constraints of an AIM mode imaging objective, key zone plate design parameters are:

Parent NA:	0.166NA
Outer zone width:	40nm
Number of zones:	2000
Focal length	0.977mm
Parent diameter:	$325\mu\text{m}$
Useable field:	$108\mu\text{m}$
Working distance:	0.97mm
Track length:	0.5m for 500x magnification

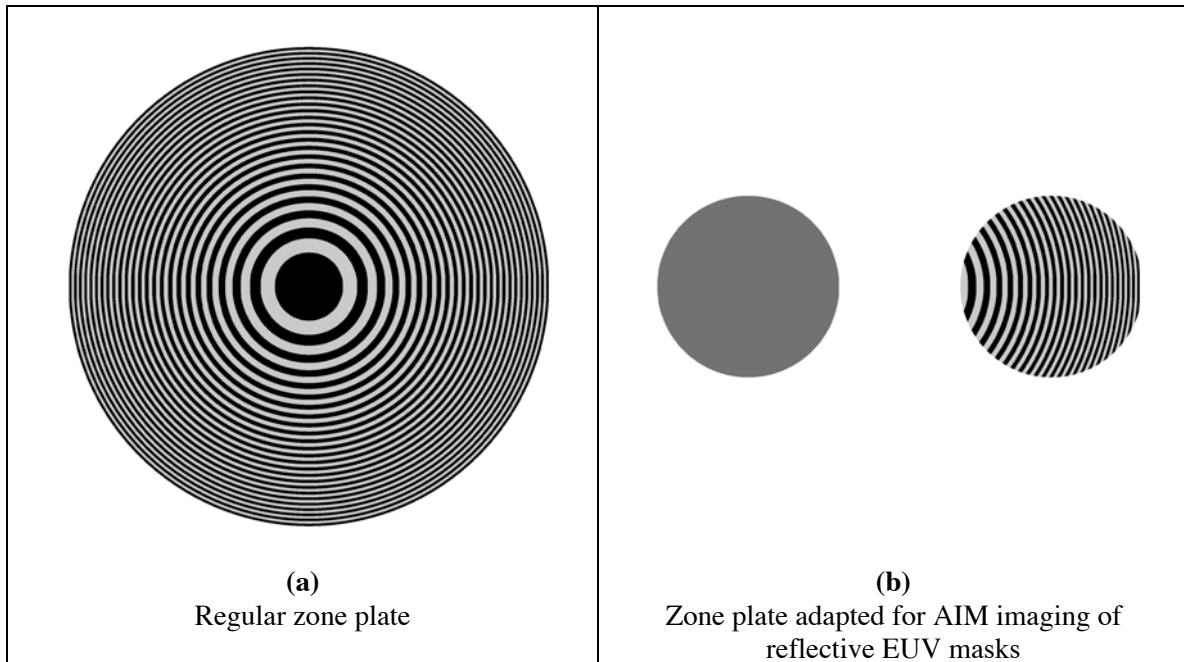
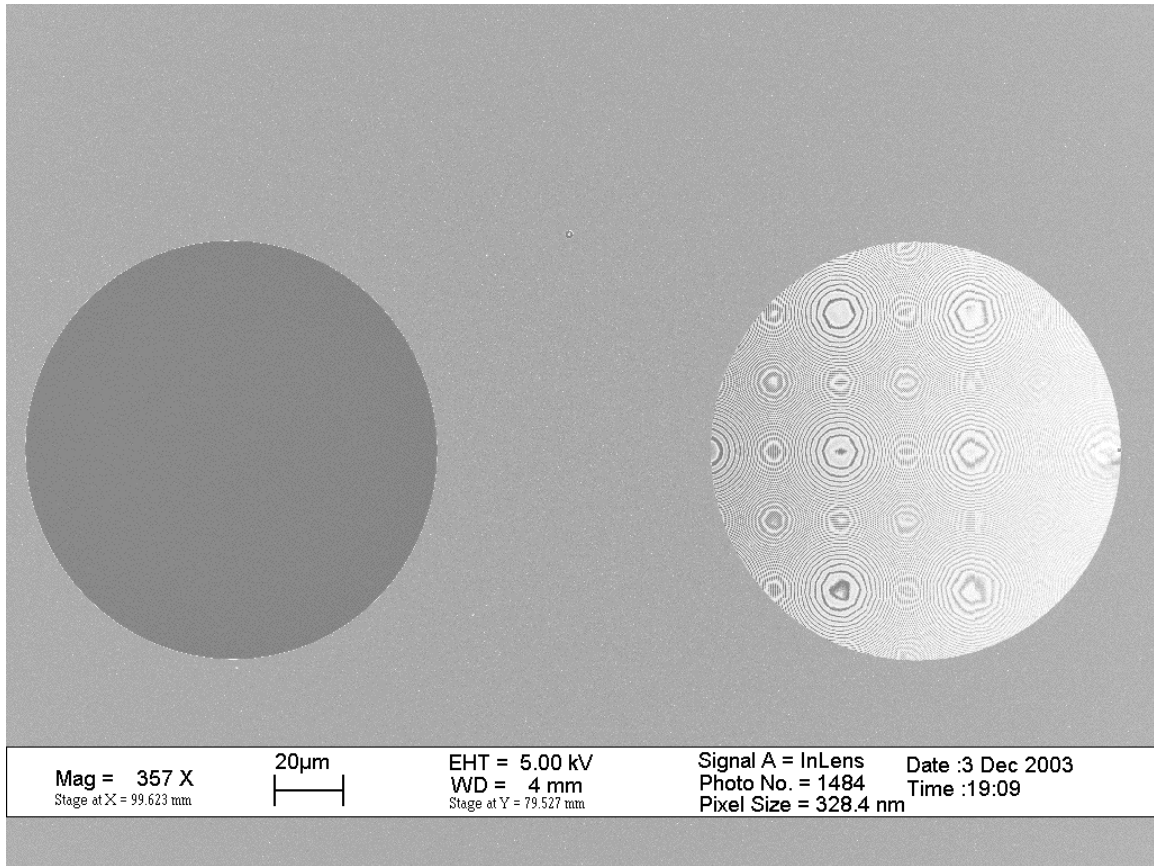


Figure 2

Zone plate design adapted for AIM mode imaging. On the left, (a), is a regular circular zone plate of the type that would be used for on-axis imaging of a transmissive sample, with $N=50$ zones for clarity. On the right, (b) is a portion of the same zone plate clipped to emulate the AIM mode pupil required for actinic inspection, plus a blank transmissive aperture through which the reflective mask can be illuminated.

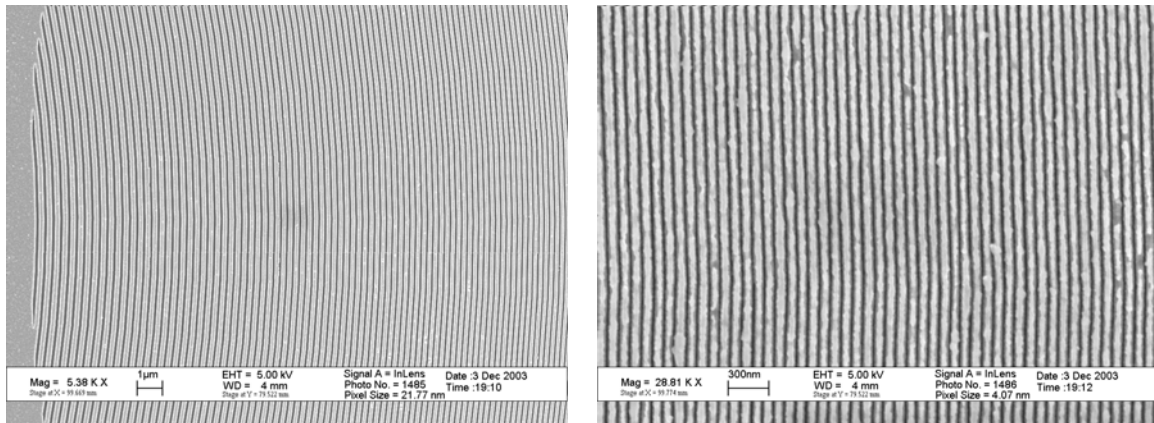
3.1.3 Zone plate fabrication

Zone plates corresponding to the above design were fabricated in the CXRO nanofabrication laboratory at Lawrence Berkeley National Laboratory. Two sets of zone plates were fabricated, one set on a transmissive Silicon Nitride membrane consists of excerpts from circular arcs as illustrated above, whilst a second set of free-standing zone plates also contains supportive spokes. The Silicon Nitride membrane absorbs EUV light, so there is loss in throughput associated with patterning on a transmissive membrane. The free standing zone plates are more fragile and more susceptible to deformation due to stress in the Nickel plating, but offers a significantly higher throughput.



(a)

Low magnification



(b)

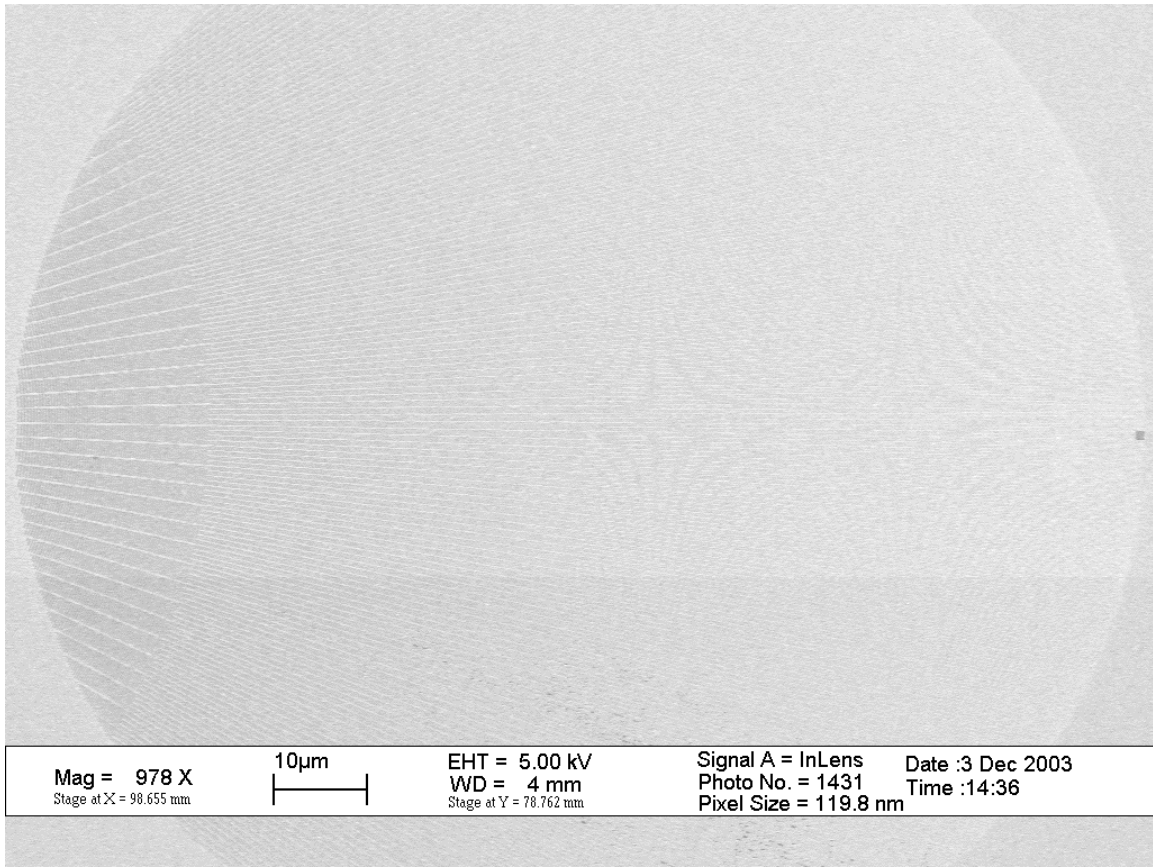
Inner edge of pattern

(c)

Outer edge of pattern

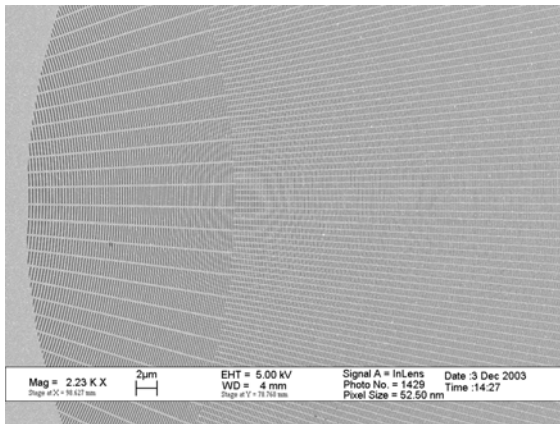
Figure 3

SEM image of zone plate patterned on Silicon Nitride membrane. (a) Low-magnification view of zone plate structure, transmissive aperture on the left and zone plate features on the right (due to line density Moiré fringes are seen in the SEM image). (b) Inner edge of the zone plate pattern and (c) outer edge seen at higher magnification. Width of the outermost zones is 40nm.



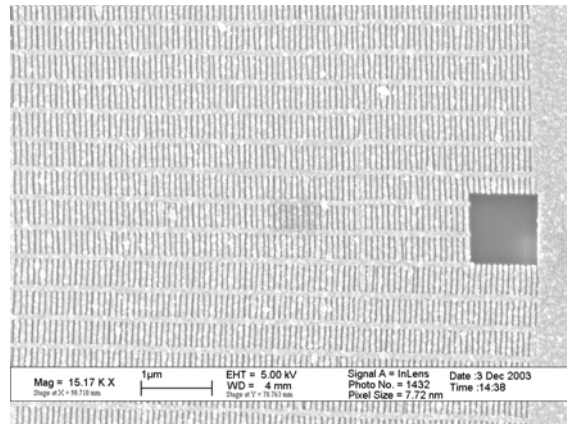
(a)

Low magnification



(b)

Inner edge of pattern



(c)

Outer edge of pattern

Figure 4

SEM image of free-standing zone plate – note the web of support structures required in order to maintain the free-standing pattern. (a) Low-magnification view of zone plate structure, transmissive aperture on the left and zone plate features on the right (due to line density Moiré fringes are seen in the SEM image). (b) Inner edge of the zone plate pattern and (c) outer edge seen at higher magnification. Width of the outermost zones is 40nm.

3.2 Imaging sub-system proof of principle demonstration

An AIM mode imaging test stand was constructed to demonstrate use of the zone plate described in Section 3.1 to image the mask optic, and risk reduction experiments conducted to demonstrate formation of an image using the zone plate optic. These experiments have been successfully completed and 80nm spatial resolution demonstrated. This resolution was obtained without any serious attempt at vibration control, and using the relatively coherent illumination (in imaging terms) provided by the bend magnet illumination. To simplify the experiment a transmissive test object was used.

3.2.1 *AIM mode imaging test stand*

An imaging test stand was constructed and installed in the reflectometer on beamline 6.3.2 at the ALS to perform the imaging system demonstration. This beamline was selected because it has a flexible multi-axis stage system for mounting the imaging system and several spare ports for mounting a CCD camera for image collection. It was therefore relatively simple to adapt the reflectometer for the purposes of performing simple imaging tests. Another factor in selection of this beamline was the availability of beamtime and staff to perform the experiments within the time window.

In order to perform these experiments it was necessary to construct a custom sample stage assembly for installation in the reflectometer, and to install a custom flange on the chamber in order to allow a CCD camera to be mounted on the chamber. The sample stage assembly holds the test pattern on an x-y-z stage, the zone plate and a fold mirror (both of which are fixed to the same baseplate). The test object is patterned on a transmissive membrane, thus the zone plate operates as a transmission microscope using the off-axis AIM pupil as will be the case in the final microscope. In order to achieve the desired angle of incidence on the sample it is necessary to tilt the sample stage assembly by 6° . A fold mirror is required in the inspection system optical path due to space restrictions under the Schwarzschild illumination optic, and this was also included in the test stand.

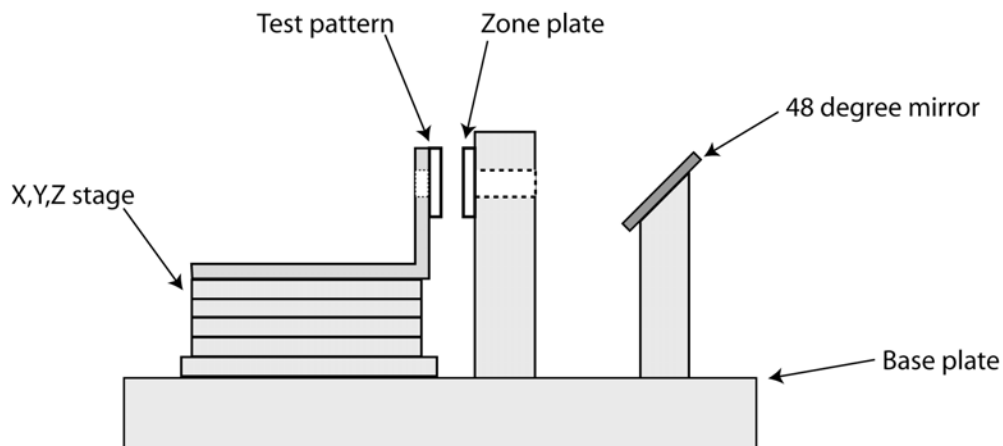


Figure 5

Schematic of the sample mount stage assembly constructed to fit into the Beamline 6.3.2. reflectometer. The distance from the sample to the zone plate is approximately 1mm. The mirror is at 48° rather than 45° because the imaging system has to be tilted at 6° to the horizontal in order to emulate the imaging conditions in the AIM microscope.

The sample stage and zone plate assembly was mounted in the reflectometer on the existing stage assembly, with a CCD camera mounted on the top of the chamber. The distance from the zone plate to the CCD is on the order of 650mm, thus the magnification is approximately 650x given the zone plate focal length of approximately 1mm. The CCD was a scientific grade Princeton Instruments CCD with 1024x1024 array of 24 μ m pixels, and a digitisation depth of 12 bits, giving an effective pixel size on the object of 40nm, and was mounted directly to the vacuum chamber without any vibration isolation.

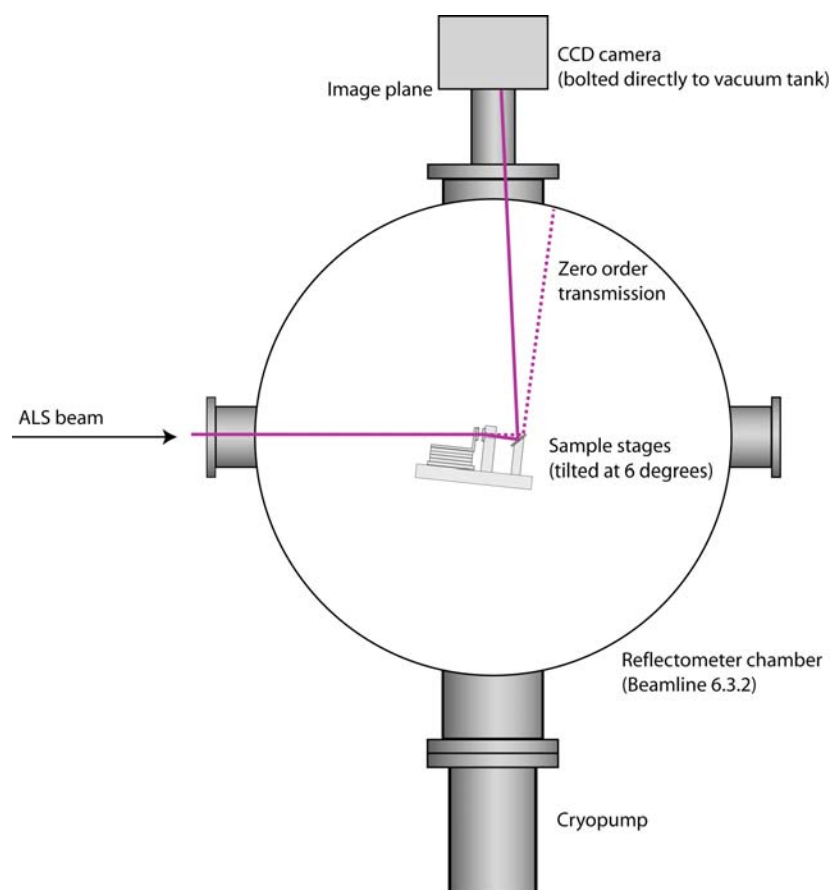


Figure 6

Installation of the imaging test stand in the Beamline 6.3.2. reflectometer at the ALS. The sample and zone plate mounting mechanism illustrated above are mounted directly onto the stage mechanism in the 6.3.2 reflectometer, and a CCD camera is bolted onto the vacuum tank. A multilayer mirror is used to fold the imaging system by 90° as will take place in the microscope being constructed for the actinic inspection system. The imaging system has to be tilted at 6° to the horizontal in order to emulate the imaging conditions in the AIM microscope.

The sample was illuminated by the focus of the reflectometer beamline optics, which image a bend magnet source into the reflectometer using Kirkpatrick-Baez mirrors to produce an elliptical illumination spot of $300 \times 100 \mu\text{m}$ with a divergence of $1.6 \times 4.3 \text{mrad}$ at the focus. This illumination corresponds to an elliptical Gaussian pupil fill of $\sigma = 0.02 \times 0.07$ with respect to the 0.0625NA pupil of the zone plate optic. The illumination is therefore relatively coherent by lithography standards, and the presence of coherence effects in the collected image is to be expected.

3.2.2 *Demonstration of imaging with resolution to 80nm dense lines*

A test pattern fabricated on a Silicon Nitride substrate was used for the imaging tests. This test pattern was microfabricated in the CXRO Nanofabrication laboratory and comprises an amplitude pattern of bright features on a dark background. The test pattern is a transmissive object selected for its variety of features, and was appropriate for testing the imaging system because the test stand design requires a transmissive object. For reference, SEM images of the test pattern are included below:

A selection of images collected using this test object is extracted in this report. In particular imaging of dense line features of 170nm , 200nm and 250nm pitch is illustrated, as is imaging of elbow patterns of 130nm and 140nm pitch. This final object is lightly out of focus, and the effects of the relatively coherent illumination can be observed.

Finally, an image of dense lines with pitch of 100nm through 50nm in 10nm increments is extracted. Line-out sections of the 90nm and 80nm dense lines are included showing the good contrast observed down to 80nm lines. Two points are worth highlighting regarding this image. First, 80nm lines on the mask correspond to 20nm printed on the wafer with a $4\times$ reduction stepper system, therefore we have digital image resolution down to features corresponding to 20nm dense lines on the wafer. Second, the Rayleigh resolution of this optic at the mask is theoretically 107nm , based on the 0.0625NA clear aperture fabricated for this zone plate to emulate the mask-side resolution of a 0.25NA , $4\times$ reduction stepper. The fact that we can image down to 80nm features at the mask is therefore encouraging and reflects well on the performance of this optic. It is particularly pleasing given the lack of vibration control associated with performing this experiment in the reflectometer.

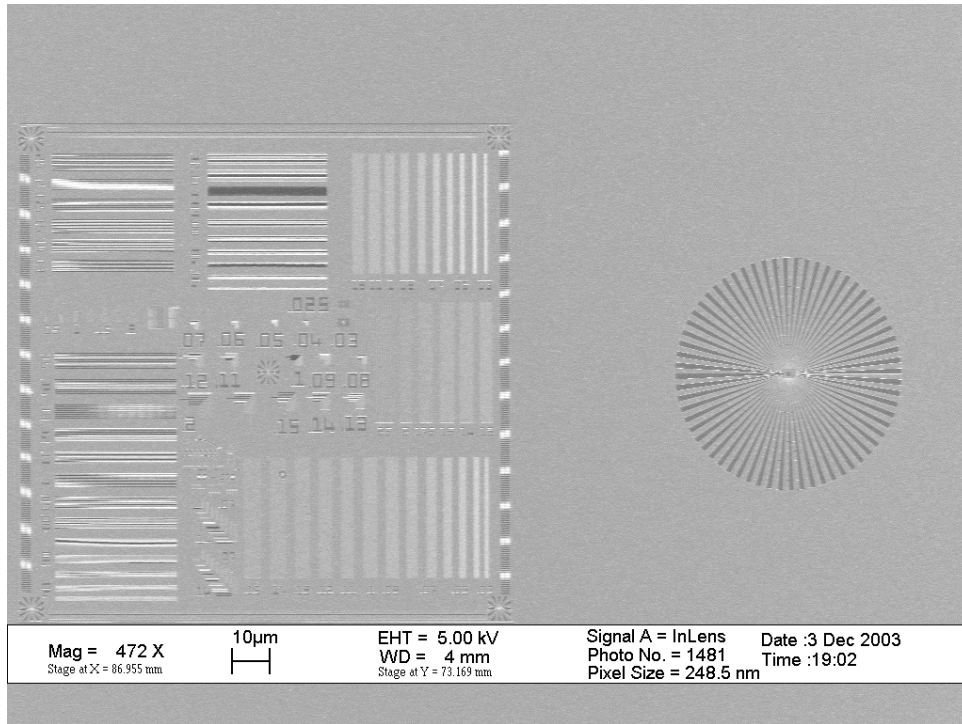


Figure 7

Low-magnification SEM picture of test pattern object.

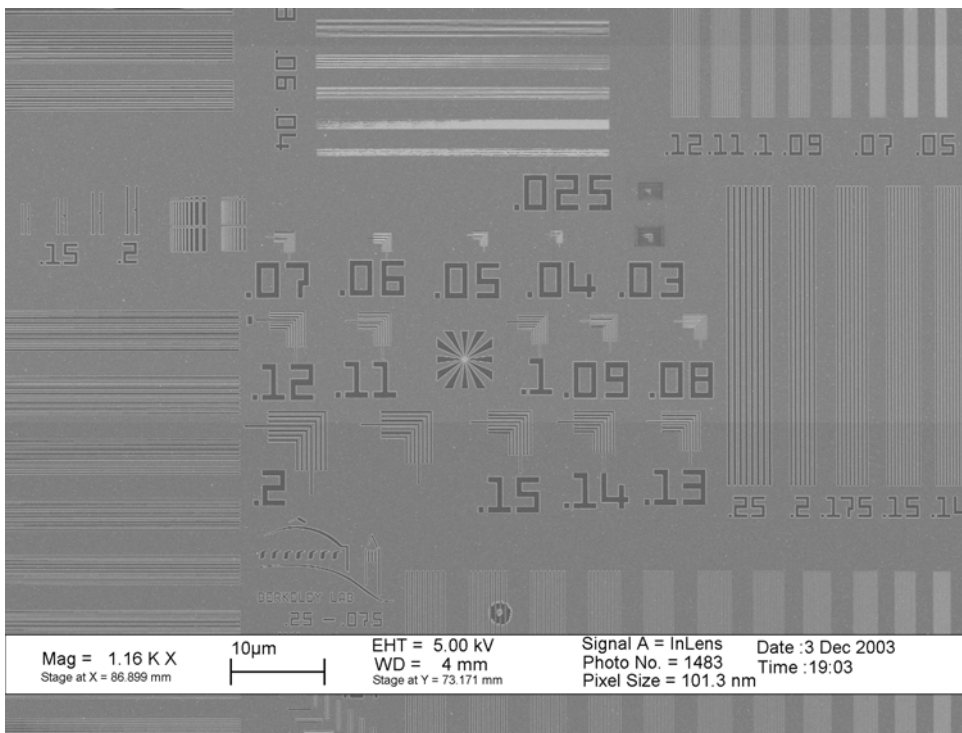


Figure 8

Higher magnification SEM view of features in the region imaged in the imaging tests.



Figure 9

Test pattern imaged using the AIM zone plate in the test stand: Dense line features of 170nm to 250nm are clearly resolved, corresponding to wafer-plane line spacings of 42 to 60nm in a 4x reduction stepper imaging system.

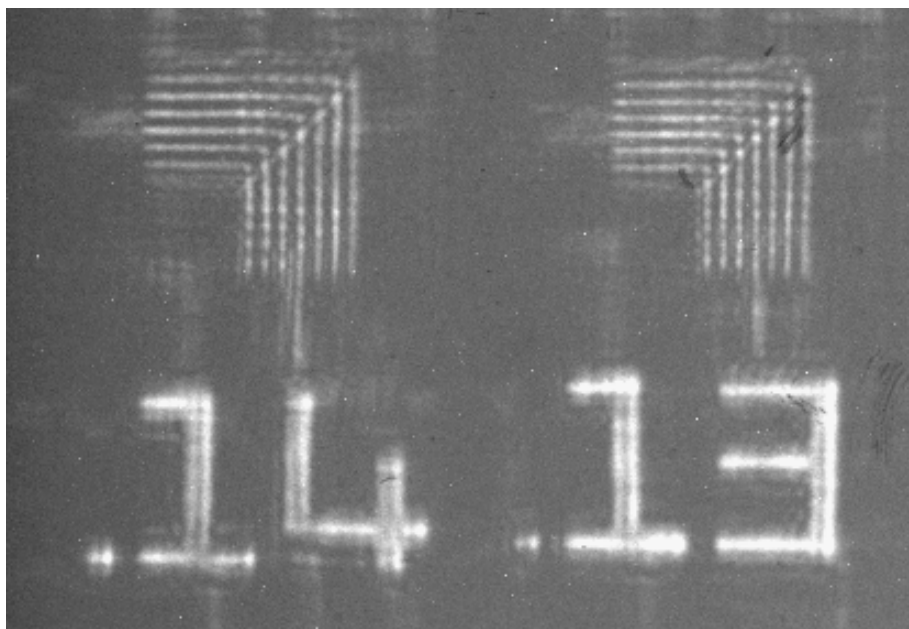
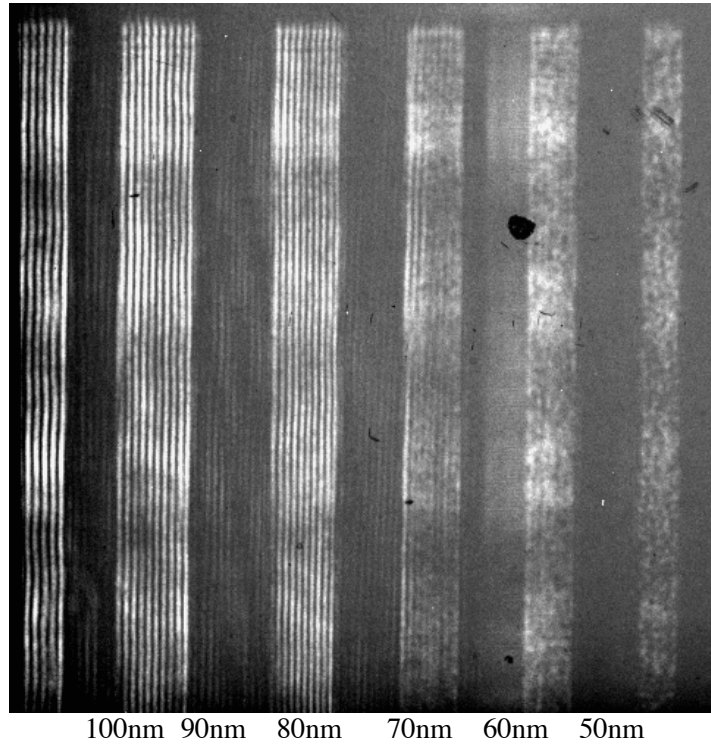


Figure 10

Test pattern imaged using the AIM test stand: 130nm elbows are resolved, even though this image is slightly out of focus. Coherence effects are also present in this image due to the relatively coherent illumination provided on the test stand beamline.



(a) Image of dense line patterns of pitch 100nm down to 50nm

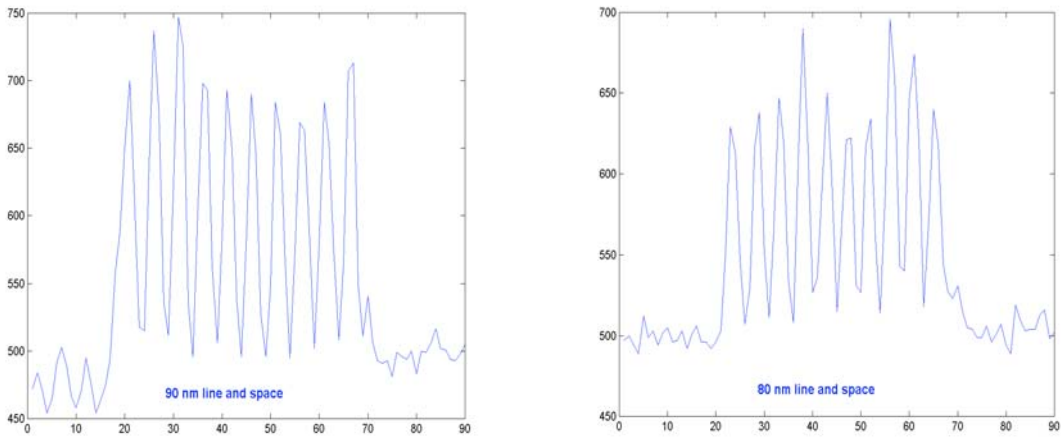


Figure 11

80nm dense lines are resolved in the test stand. Line width from left to right is 100nm, 90nm, 80nm, 70nm, 60nm and 50nm. Lineouts of 90nm and 80nm images show that these features are clearly resolved. Theoretical resolution of this zone plate is 107nm, as determined by the 0.0625NA clear aperture of the optic design. Feature sizes are at the mask – assuming 4x reduction 80nm features on the mask correspond to 20nm lines on the wafer.

3.3 10x optic demonstration

A test stand was fabricated and installed on beamline 11.3.2 to verify the performance of the Schwarzschild optic in the configuration to be used in the final scanning system. Risk reduction tasks were performed to demonstrate the throughput and spot size achievable with the optic with a view to verifying its compatibility with the requirements of the project.

3.3.1 *Hardware fabrication and installation*

The following modifications were required in order to perform the risk reduction tasks on Beamline 11.3.2 at the ALS.

1. **Modifications to pinhole chamber**

The proposed inspection system design requires the optics to be located below the pinhole chamber, whereas the previous inspection system had the inspection system located in-line with the pinhole chamber. A fold mirror assembly was therefore constructed and installed in the pinhole chamber to redirect the ALS beam down into the Schwarzschild optic. The fold mirror is located behind the pinhole, so that the flux incident on the mirror is only that portion of the beam that passes through the pinhole. In addition to redirecting the ALS beam, the fold mirror also provides bandwidth selection when the beamline is run in “white light” mode without the monochromator. The mirror is relatively easily changed and eminently replaceable should it become contaminated as a result of being illuminated by the full bandwidth of the ALS. This fold mirror assembly will be used in the final inspection system as well as in these risk reduction experiments.

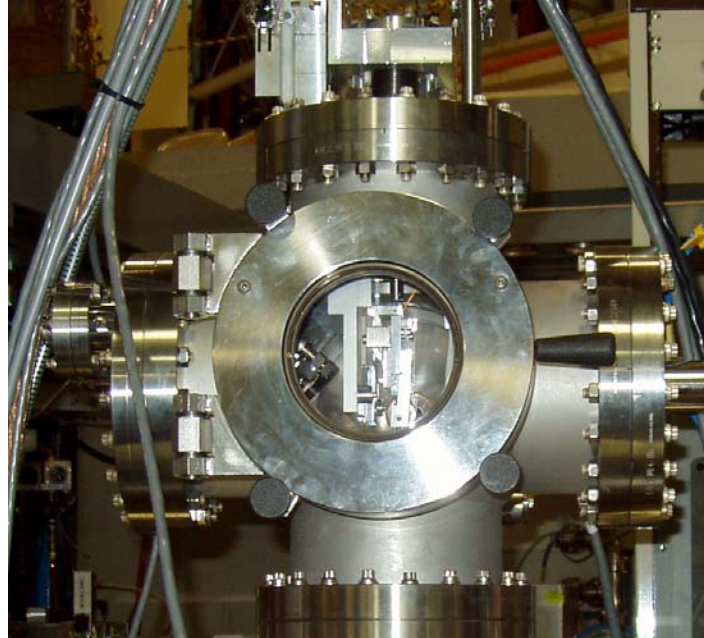


Figure 12

Fold mirror assembly located in the pinhole chamber to redirect ALS beam into the Schwarzschild optic, which is located below the pinhole chamber. The fold mirror is just visible behind the pinhole stages in the above photograph.

2. Temporary end-station for risk reduction experiments.

A temporary vacuum chamber was constructed to house the Schwarzschild optic and stages for the throughput and knife-edge tests, including decks and mounting hardware to hold the optics and stage mechanism. This chamber was installed and aligned on the actinic inspection beamline at the ALS in December 2003. The chamber and optics are illustrated in the photographs below. This temporary end-station will be replaced with the final integrated inspection system once fabrication of the inspection system hardware is complete.

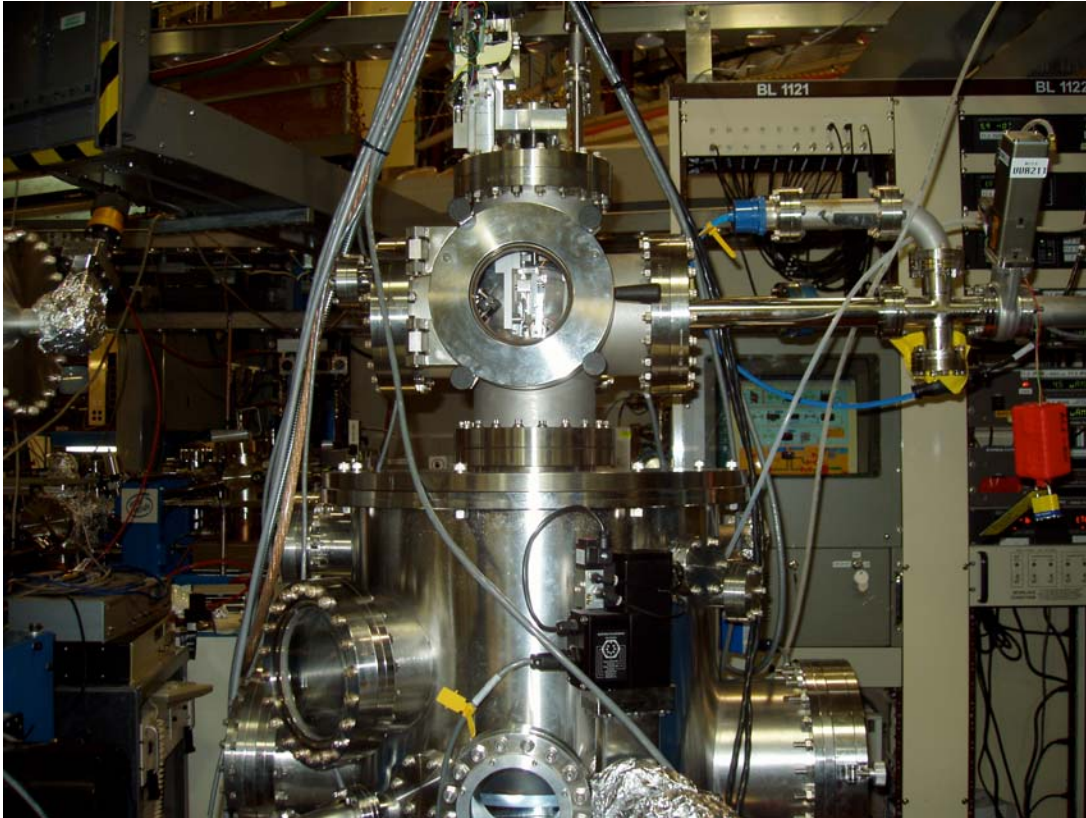


Figure 13

Test stand end station installed on beamline 11.3.2 to demonstrate performance of the Schwarzschild optic in the configuration to be used in the final scanning system.

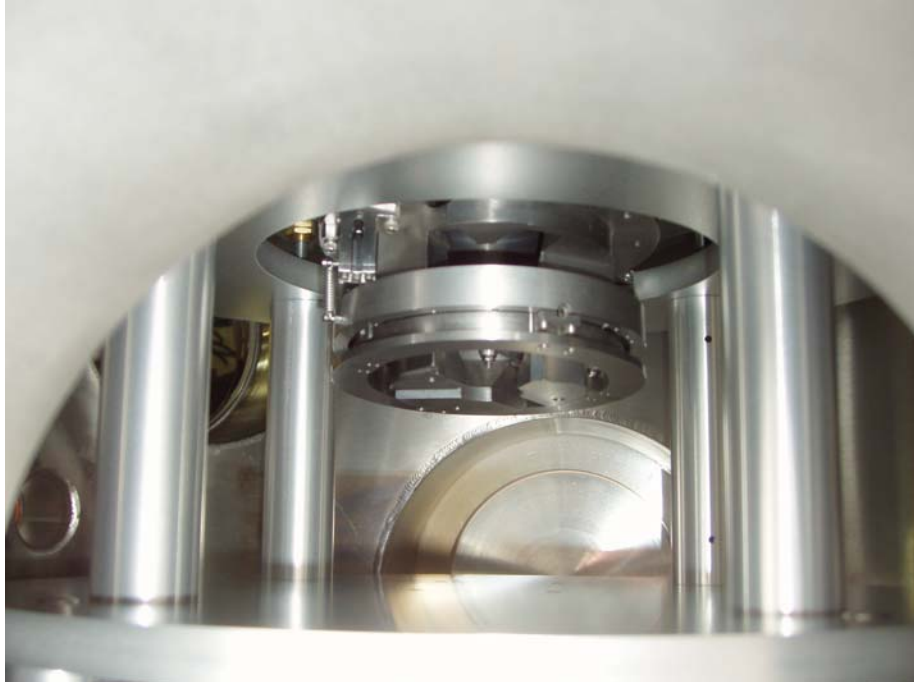


Figure 14

Schwarzschild optic installed in the test stand. Stages for the knife-edge test are installed on the deck visible in the photo, but are not shown in this photo for the sake of clarity. The optic focus is located approximately 25mm below the base of the optic housing.

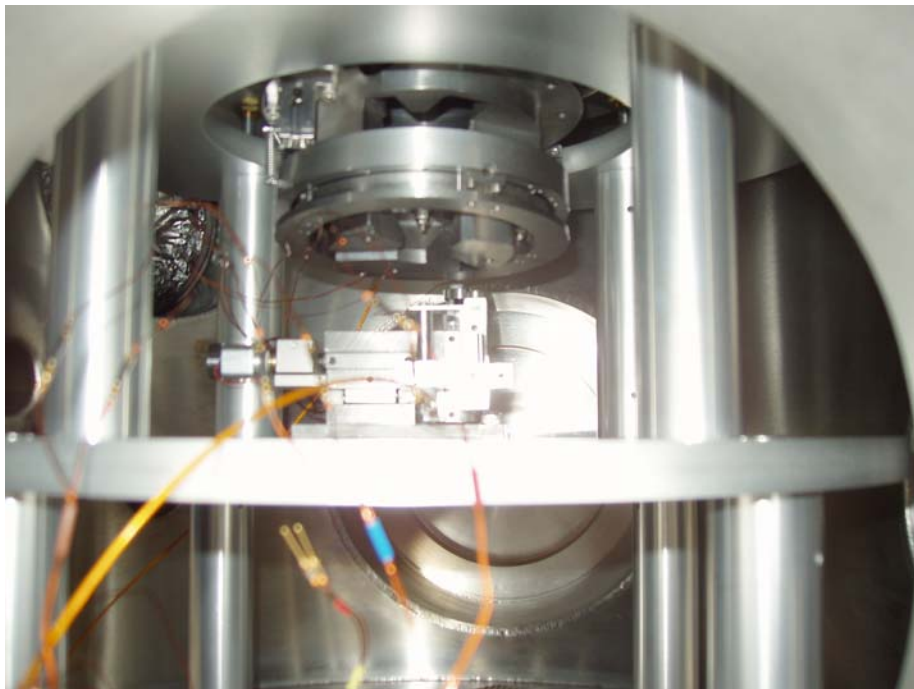


Figure 15

Stages for the knife edge scan installed in the test chamber.

3.3.2 Measurement of system throughput

Total system throughput has been measured for the imaging system by measuring the flux incident on a photodiode located near the system focus. The measured throughput therefore incorporates the reflectivity of the fold mirror, the Schwarzschild throughput, and a factor dependent on wavelength matching between the two multilayer coated optics. Proper characterisation of the fold mirror is therefore critical to assessing overall system performance.

Fold mirror performance was measured in the ALS reflectometer both with and without the order sorter present. It is important to note the difference between these two measurements. Unlike the reflectometer, the actinic inspection beamline does not have an order sorter in the optical path. Higher order harmonics of the monochromator are incident on the pinhole, thus the light reflected into the Schwarzschild relative to the flux immediately behind the pinhole is given by the reflectivity measured without the order sorter.

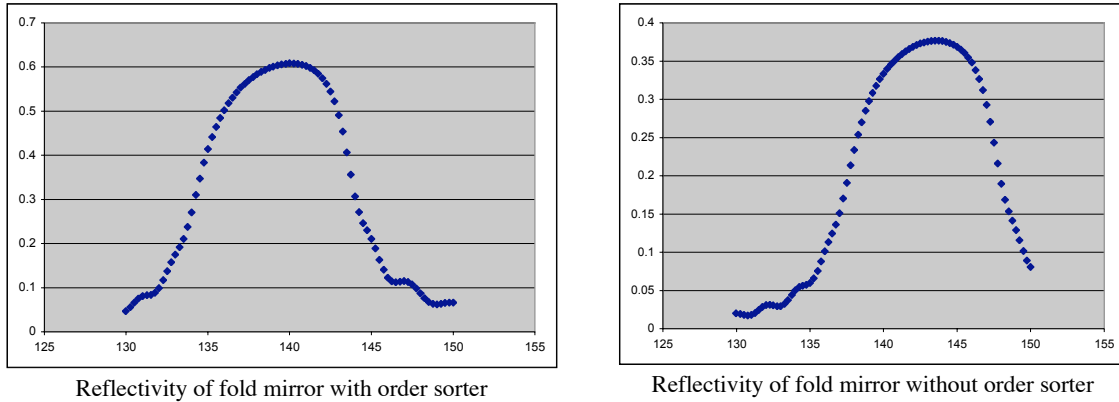


Figure 16

Left: Measured reflectivity of the fold mirror performance as a function of wavelength at the 42° angle of incidence used in the actinic inspection system. The mirror consists of a Mo/Si multilayer with a period of 10nm.

Right: Measured reflectivity of the same multilayer with no order sorter in place. Unlike the reflectometer on beamline 6.3.2 the actinic inspection beamline does not have an order sorter, therefore this reflectivity curve therefore represents difference between flux measured immediately behind the pinhole and flux reflected into the Schwarzschild optic in the actinic inspection system.

The characterised fold mirror was installed in the pinhole chamber on the actinic inspection beamline and throughput measurements made of the combined Schwarzschild and fold mirror system as a function of wavelength. Peak system throughput was measured to be 2.2% at 13.5nm, however a significant wavelength mismatch was observed between the Schwarzschild and fold mirror that reduced throughput. Normalising for the previously measured reflectivity of the fold mirror as a function of wavelength it is possible to infer the throughput of the Schwarzschild alone. This calculation yields a peak throughput of the Schwarzschild optic of 37% at 13.35nm, corresponding to an individual mirror reflectivity of 60.9% for this two mirror system and within the expected bounds for this optic. This data is presented graphically in the following figures.

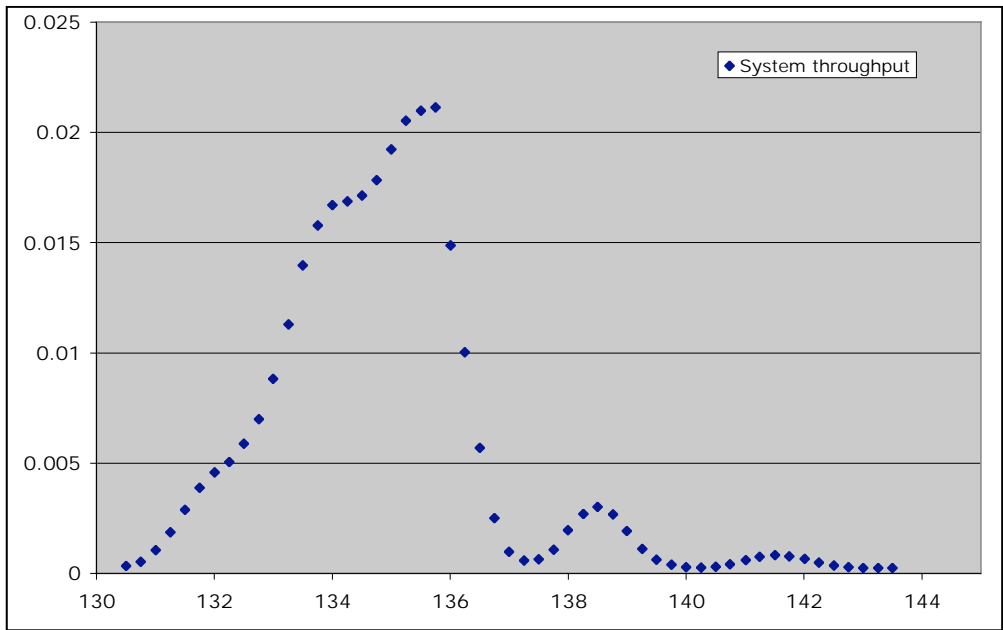


Figure 17

Combined system throughput of fold mirror and Schwarzschild optic.

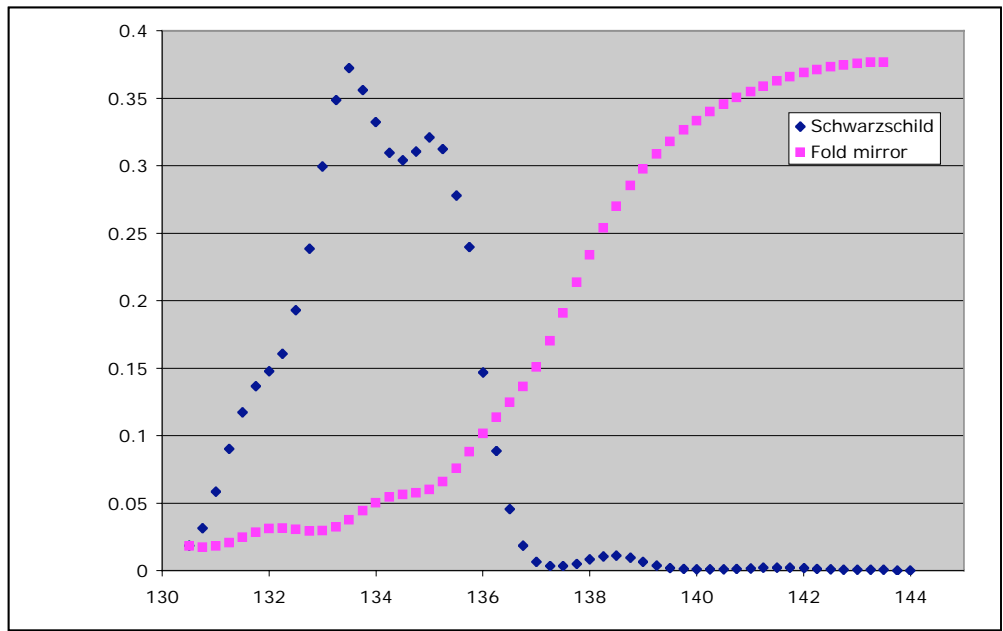


Figure 18

Throughput of the Schwarzschild optic inferred from the known reflectivity of the fold mirror. The peak Schwarzschild throughput is measured to be 37%, corresponding to an individual mirror reflectivity of 60.8% for the two optic system. The wavelength mismatch between the fold mirror and Schwarzschild can be easily corrected by installing a fold mirror manufactured to match the wavelength characteristics of the Schwarzschild optic, potentially improving overall system throughput by factor of 10 or more over the measurements made here.

Fortunately, it is relatively simple to correct for the throughput hit caused by the wavelength mismatch between the fold mirror and the Schwarzschild: it is simply necessary to produce a new fold mirror matched in wavelength to the measured peak transmission of the Schwarzschild. The fold mirror is a plane mirror consisting of a 1" square segment from a multilayer coated Silicon wafer, therefore it is relatively easy and cheap to produce another mirror specifically for this purpose.

3.3.3 Knife-edge tests of spot size

Knife-edge scans have been performed on the focal spot produced by the Schwarzschild optic in the test stand and the focal spot characterised. A $20\mu\text{m}$ pinhole was inserted into the beam path in the pinhole chamber to produce a focal spot of approximately $1\mu\text{m}$ given the nominal 20x magnification of the optical system. A knife-edge was mounted on an XYZ translation stage and scanned through the focal region at a known speed whilst the photodiode current was simultaneously measured. The data was logged to produce a plot of the intensity variation as the knife-edge is scanned through the focal spot. To achieve focus, the scan was repeated whilst manually adjusting the Z-axis height of the knife edge to produce the sharpest transition in intensity as a function of position. The data presented here indicate the best results achieved to date in the period of time between 18 and 21 December 2003. The focal spot size is measured to be close to $1\mu\text{m}$ FWHM as expected.

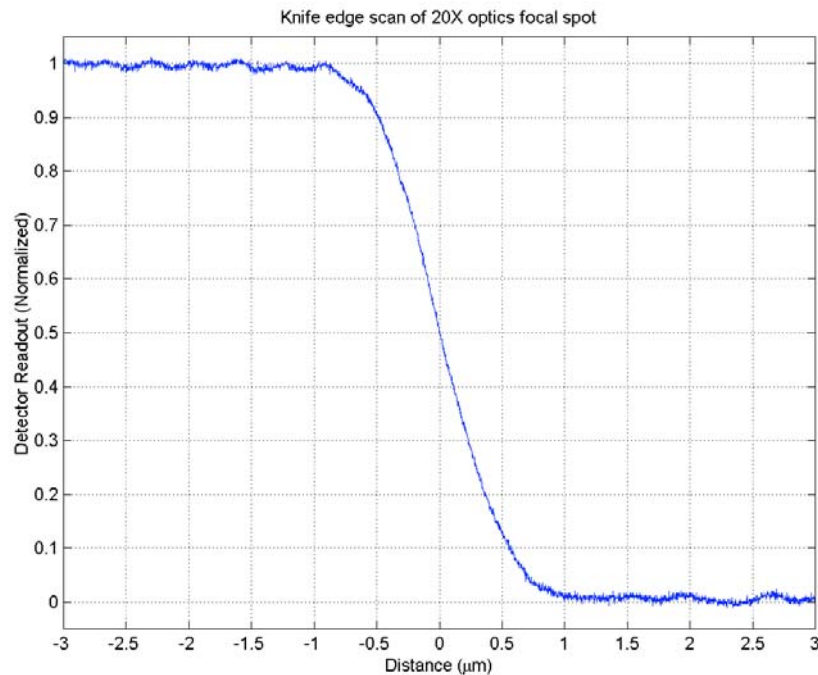


Figure 19

Knife-edge scan of the Schwarzschild focal spot when imaging a $20\mu\text{m}$ pinhole. The 10% to 90% intensity threshold lies within a $1\mu\text{m}$ region, indicating that a $1\mu\text{m}$ spot size has been formed as expected.

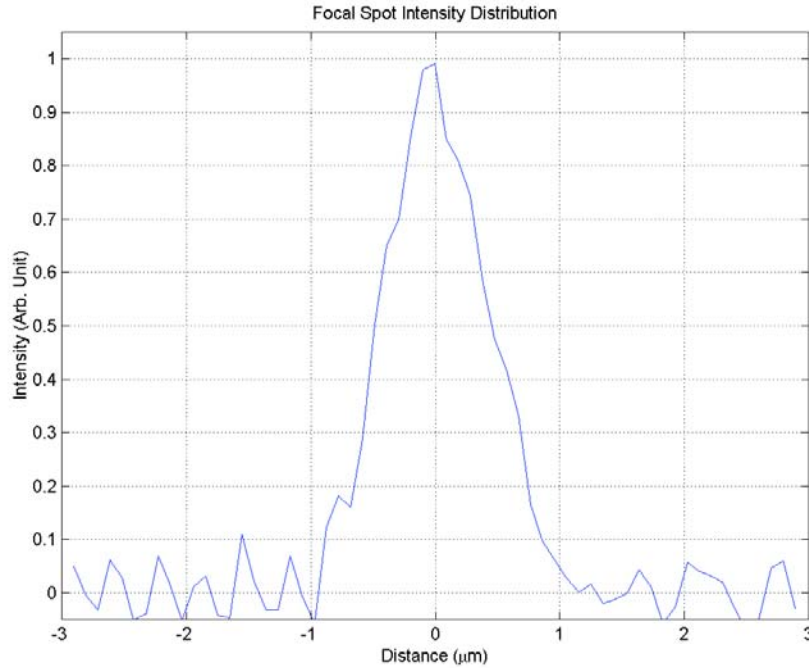


Figure 20

Derivative of the knife-edge scan, which gives an indication of the intensity profile across the focal spot. Note that the focal spot is circular in shape and that the $20\mu\text{m}$ pinhole is imaged to a spot approximately $1\mu\text{m}$ in size, therefore even for ideal optic performance this derivative would not have perfectly sharp edges.

Note that this measurement is taken at best focus obtained with the optic in its current alignment state, and that the object may not currently be located in the best field point. There may therefore be room for improvement in spot size performance as alignment of the Schwarzschild to the rest of the beamline is optimised. It is also possible that clocking the optic may improve performance by moving the illuminated patch to a better pupil on the mirror surface.

3.4 Data acquisition system and electronics

The ability to continuously collect and store two channels of analogue data at speed of 100kHz or greater is required in order to meet the target scan speed of the inspection project. We have acquired data acquisition hardware capable of running at the required data acquisition speed and have demonstrated continuous acquisition of two channels of data at speeds of up to 500kHz for intervals in excess of 5 minutes continuous readout. Analysis of the data stream shows that the data acquisition system is capable of simultaneously sampling two streams of data and saving the data to disk.

Currently the limiting factor on acquisition rate is computer speed, and we found no limit to acquisition time other than available disk space. Note that these tests were performed using a 400Mhz Pentium II PC to control data acquisition and storage, which has been demonstrated to be capable of meeting the requirements of the project. We have demonstrated that real-time data

acquisition and storage is no longer a major risk item for the project, and anticipate the ability to go to higher data rates if required using faster computer hardware.

3.4.1 Overview of data acquisition system

Two channels of data are simultaneously acquired from the bright-field and dark-field detectors by a PXI 6115 ADC converter and saved to disk in real time. External timing signals are used to synchronise data acquisition with movement of the stages and, therefore, motion of the sample under the scanning optics. This data collection arrangement is illustrated below.

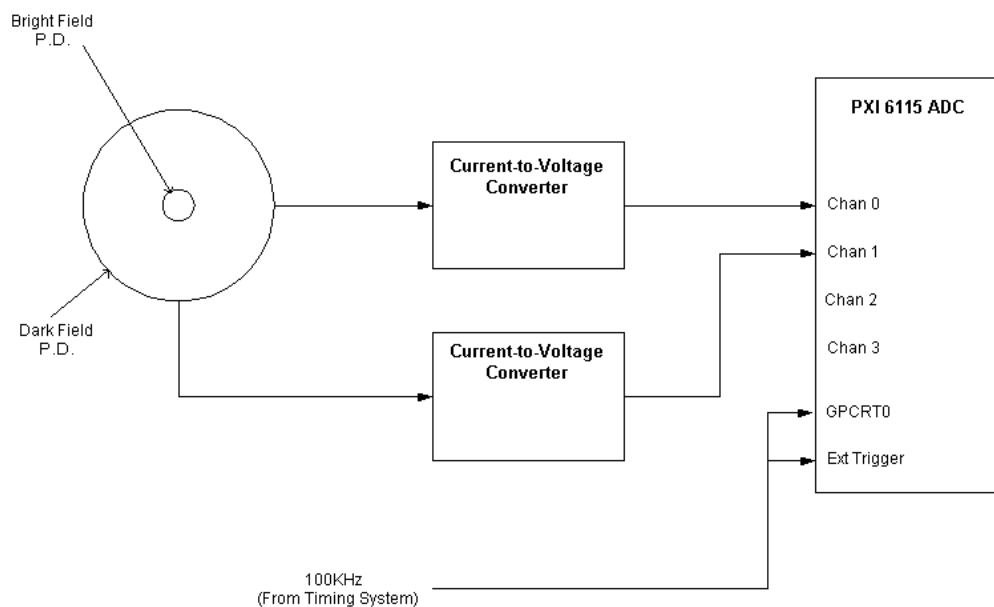


Figure 21

Overview of data acquisition system. Two channels of data are simultaneously acquired from the bright-field and dark-field detectors by a PXI 6115 ADC converter and saved to disk in real time. External timing signals are used to synchronise data acquisition with movement of the stages and, therefore, motion of the sample under the scanning optics.

For the final end-station data acquisition system it is necessary to interface the data acquisition hardware to the stage and motion system of the end-station being constructed by Rohwedder. It is necessary to be able to interrupt the scan system, for example in the case of loss of beam, and additional data must be collected from the stages regarding sample position and machine state. These are illustrated schematically below.

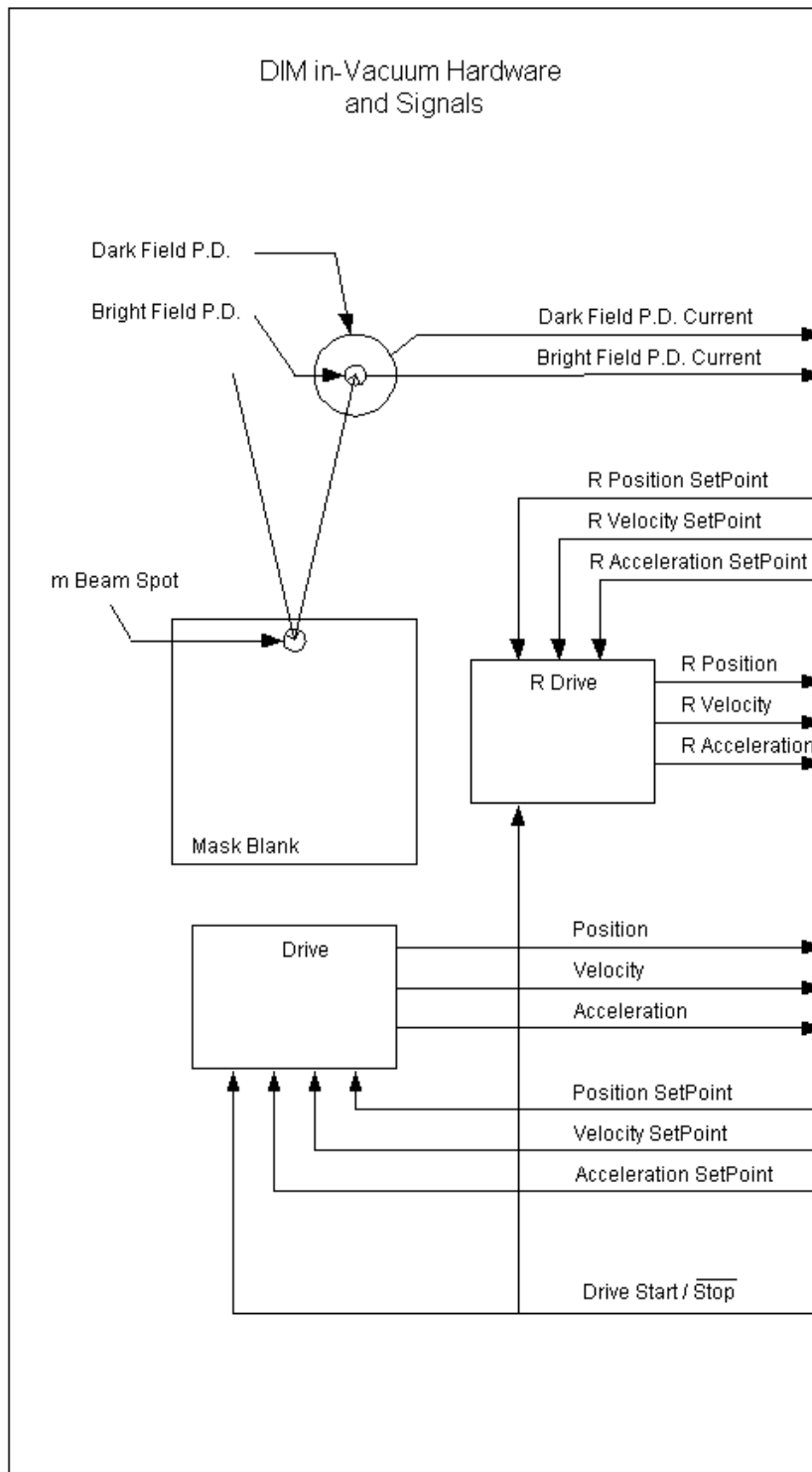


Figure 22

Overview of interaction between data acquisition system and Rohwedder controls system.

3.4.2 Demonstration of continuous real-time data acquisition

To demonstrate the real-time data archiving capability of the data acquisition system at the required data storage rate we continuously acquired a 10kHz waveform for a period of 5 minutes at 200kHz and analysed the data for synchronisation and drift between the two channels, and any dropouts in data archiving. No dropouts were observed during the data acquisition period, and the ADC maintained synchronisation between the two channels of data throughout the data collection period.

Segments of the data stream are extracted and plotted below, illustrating performance of the ADC unit in real-time data acquisition mode.

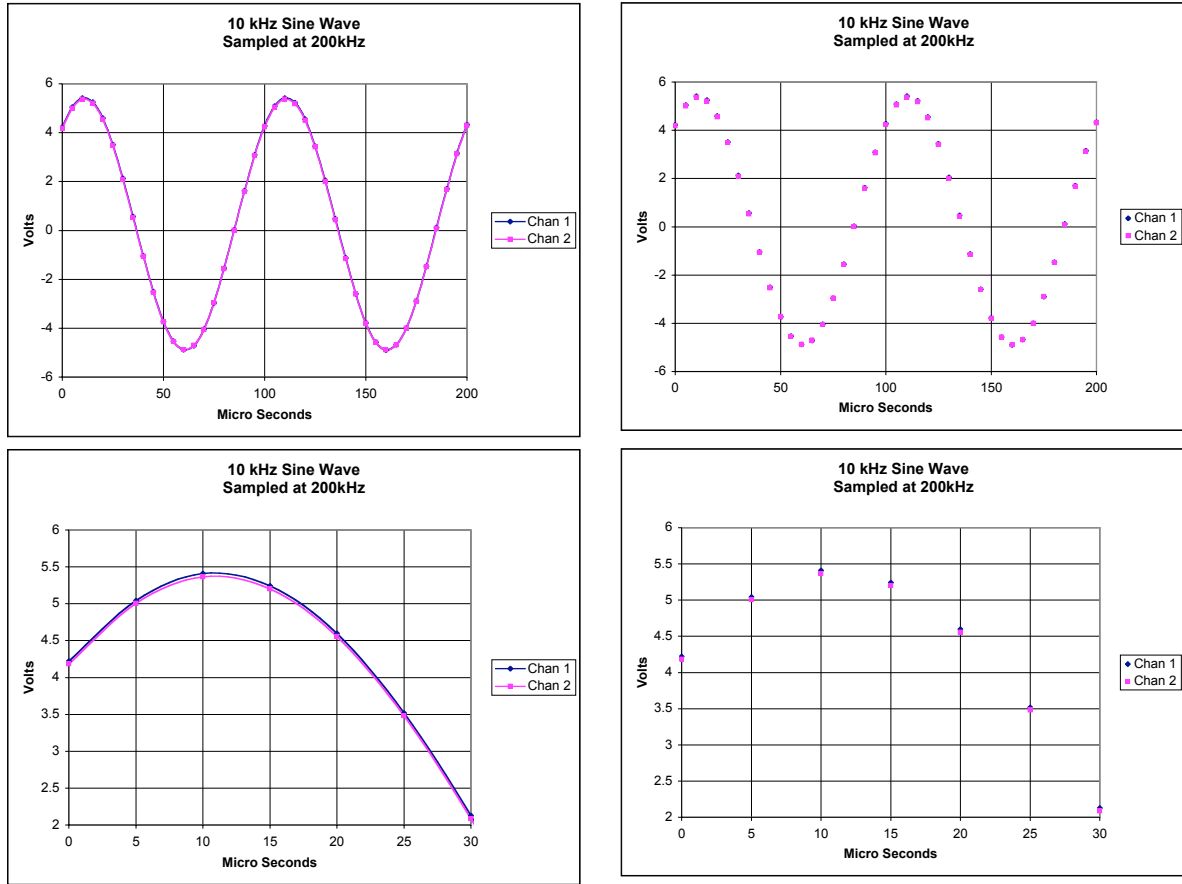


Figure 23

Sample of data continuously acquired for a period of 5 minutes. Synchronisation of data is maintained throughout the data set, and no drift is observed between the two ADC units indicating that the system is truly simultaneously sampling the input data.

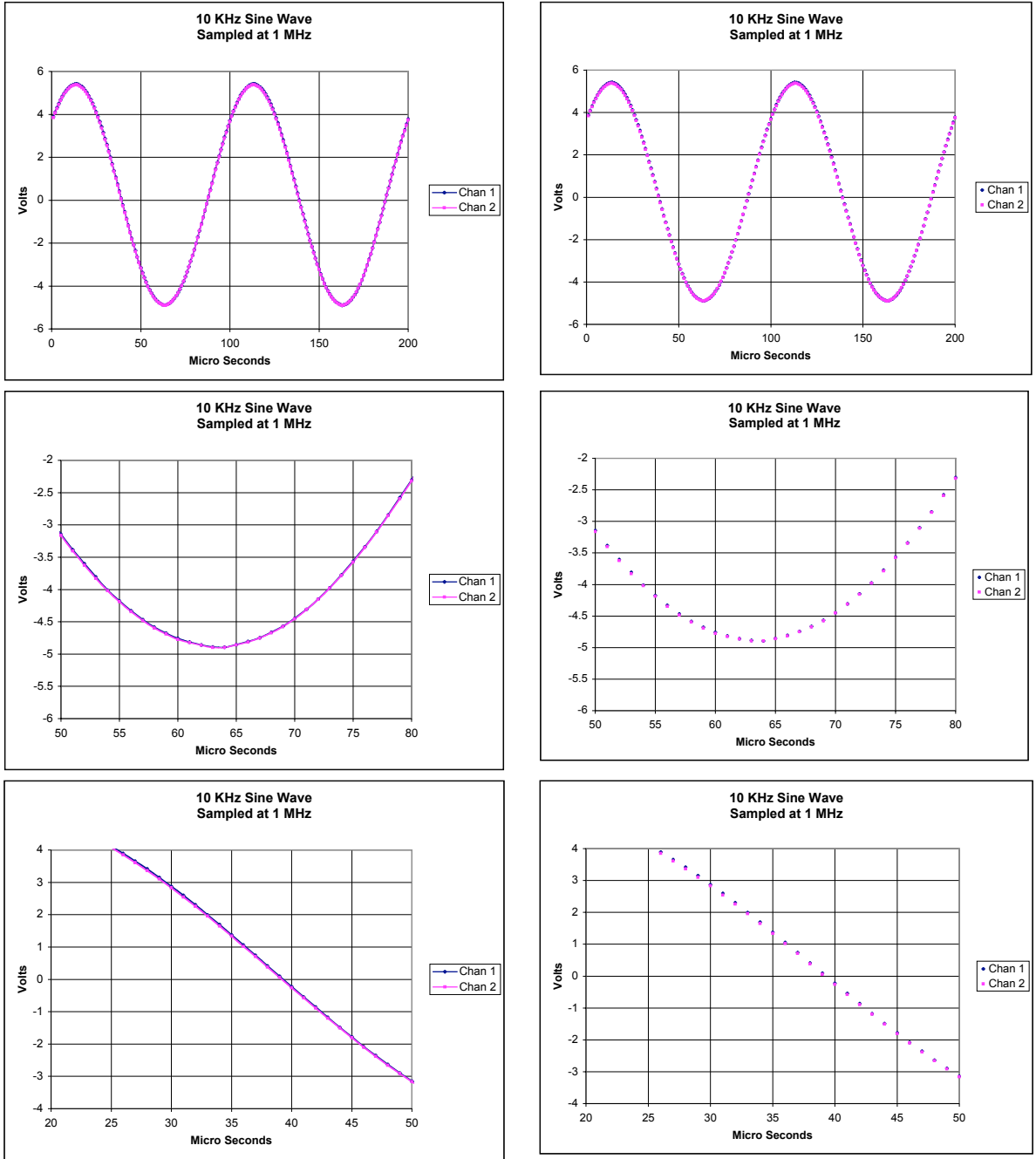


Figure 24

Simultaneous data acquisition at 1MHz illustrating that the acquisition system remains synchronised at this data rate. The target acquisition speed for the actinic inspection system is 100kHz, therefore this data indicates at least a factor of 10x headroom in sampling rate capability.